

Membrane Binding of HIV-1 Matrix Protein: Dependence on Bilayer Composition and Protein Lipidation

Marilia Barros,^a  Frank Heinrich,^{a,c}  Siddhartha A. K. Datta,^d Alan Rein,^d  Ioannis Karageorgos,^{e,f} Hirsh Nanda,^{a,c,*}  Mathias Lösche^{a,b,c}

Department of Physics^a and Department of Biomedical Engineering^b, Carnegie Mellon University, Pittsburgh, Pennsylvania, USA; NIST Center for Neutron Research, National Institute of Standards and Technology, Gaithersburg, Maryland, USA^c; HIV Dynamics and Replication Program, Center for Cancer Research, National Institute of Cancer, Frederick, Maryland, USA^d; Biomolecular Measurement Division, National Institute of Standards and Technology, Gaithersburg, Maryland, USA^e; Institute for Bioscience and Biotechnology Research, Rockville, Maryland, USA^f

ABSTRACT

By assembling in a protein lattice on the host's plasma membrane, the retroviral Gag polyprotein triggers formation of the viral protein/membrane shell. The MA domain of Gag employs multiple signals—electrostatic, hydrophobic, and lipid-specific—to bring the protein to the plasma membrane, thereby complementing protein-protein interactions, located in full-length Gag, in lattice formation. We report the interaction of myristoylated and unmyristoylated HIV-1 Gag MA domains with bilayers composed of purified lipid components to dissect these complex membrane signals and quantify their contributions to the overall interaction. Surface plasmon resonance on well-defined planar membrane models is used to quantify binding affinities and amounts of protein and yields free binding energy contributions, ΔG , of the various signals. Charge-charge interactions in the absence of the phosphatidylinositide PI(4,5)P₂ attract the protein to acidic membrane surfaces, and myristoylation increases the affinity by a factor of 10; thus, our data do not provide evidence for a PI(4,5)P₂ trigger of myristate exposure. Lipid-specific interactions with PI(4,5)P₂, the major signal lipid in the inner plasma membrane, increase membrane attraction at a level similar to that of protein lipidation. While cholesterol does not directly engage in interactions, it augments protein affinity strongly by facilitating efficient myristate insertion and PI(4,5)P₂ binding. We thus observe that the isolated MA protein, in the absence of protein-protein interaction conferred by the full-length Gag, binds the membrane with submicromolar affinities.

IMPORTANCE

Like other retroviral species, the Gag polyprotein of HIV-1 contains three major domains: the N-terminal, myristoylated MA domain that targets the protein to the plasma membrane of the host; a central capsid-forming domain; and the C-terminal, genome-binding nucleocapsid domain. These domains act in concert to condense Gag into a membrane-bounded protein lattice that recruits genomic RNA into the virus and forms the shell of a budding immature viral capsid. In binding studies of HIV-1 Gag MA to model membranes with well-controlled lipid composition, we dissect the multiple interactions of the MA domain with its target membrane. This results in a detailed understanding of the thermodynamic aspects that determine membrane association, preferential lipid recruitment to the viral shell, and those aspects of Gag assembly into the membrane-bound protein lattice that are determined by MA.

The polyprotein Gag is an essential component for the reproduction of retroviruses, such as HIV-1, in infected cells. In the production of new viruses, many copies of Gag assemble laterally, either in the cytoplasm or on the plasma membrane (PM) of the host, thus acquiring their lipid envelope as they bud from the cell. Distinct retroviral genera encode Gag proteins which all show a similar domain architecture, with an N-terminal matrix (MA) domain that targets the PM, followed by the capsid (CA) and nucleocapsid (NC) proteins that are connected by minor domains or unstructured peptide linkers. Across retroviral genera, MA domains also share a high degree of structural homology (1). Most of their N-terminal portions comprise five or six α -helices and adopt a compact globular fold, whereas their C termini are often flexible or unstructured (2). Moreover, retroviral MA domains share electrostatic homology: basic amino acids are clustered on one surface of their N-terminal “globular heads,” resulting in a basic patch that interacts electrostatically with the PM of the infected cell (3). On the other hand, the MA domains of different retroviruses differ in their net charges in this basic patch, which suggests differing contribution of electrostatic interactions in the targeting of these

proteins. They also differ in cotranslational modifications, since some, such as HIV-1 MA, are lipidated whereas those of others, such as Rous sarcoma virus (RSV), are not. Both the myristoylation of HIV MA and its basic patch are required for correct PM targeting (4, 5). Indeed, Gag protein that included an MA-Src chimera in which the first 31 MA residues were replaced by the N-terminal end of Src was found to bind membranes and form

Received 5 November 2015 Accepted 15 February 2016

Accepted manuscript posted online 24 February 2016

Citation Barros M, Heinrich F, Datta SAK, Rein A, Karageorgos I, Nanda H, Lösche M. 2016. Membrane binding of HIV-1 matrix protein: dependence on bilayer composition and protein lipidation. *J Virol* 90:4544–4555.
doi:10.1128/JVI.02820-15.

Editor: W. I. Sundquist

Address correspondence to Alan Rein, reina@mail.nih.gov, or Mathias Lösche, quench@cmu.edu.

* Present address: Hirsh Nanda, Janssen, LLC, Spring House, Pennsylvania, USA.

Copyright © 2016, American Society for Microbiology. All Rights Reserved.

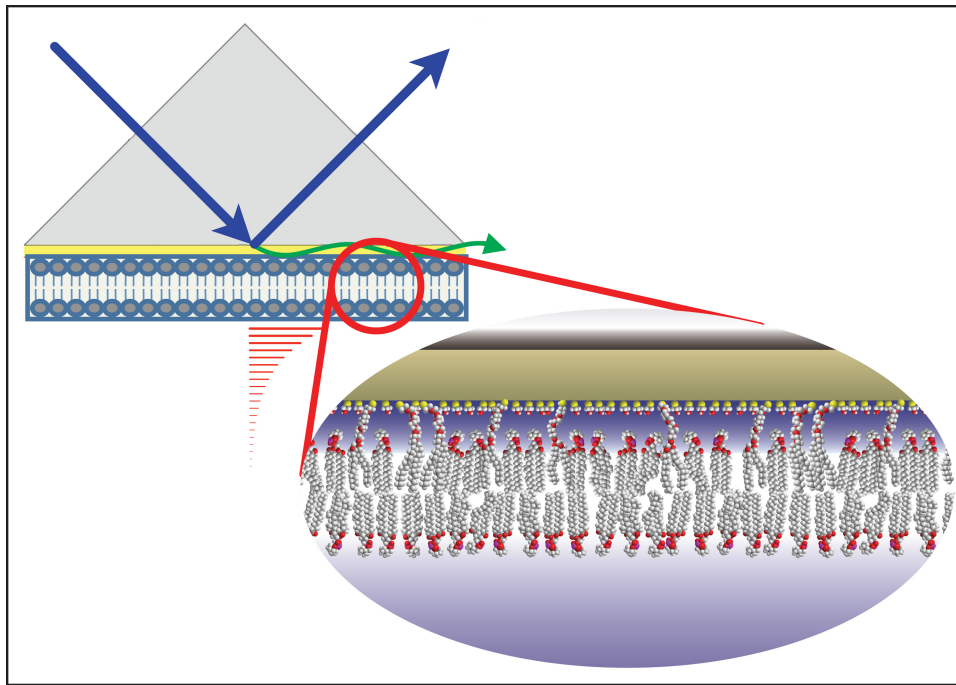


FIG 1 Schematic representation of the experimental configuration of the SPR measurements on an stBLM. The ultrathin gold layer on a glass substrate is passivated by a densely packed mercaptoethanol layer on which the membrane is grafted. The surface-ligated bilayer is highly hydrated at both interfaces and in-plane fluid, and yet resilient to experimental manipulation, and virtually defect-free. Its lipidic composition can be precisely controlled.

virus-like particles with the same characteristic dependence on basic residues and myristoylation as native HIV Gag (4). Although only MA is in direct contact with the surrounding membrane in the completed viral shell, the remaining domains of the Gag poly-protein contribute to Gag membrane affinity. It is well documented that CA-CA interactions drive Gag oligomerization (6, 7), and artificial multimerization of MA enhances its affinity to membranes by an order of magnitude (8). Moreover, a recent study identifies protein-protein contacts in the SPA segment of RSV Gag that stabilize oligomers and increase membrane affinity, leading in turn to pronounced cooperativity in membrane binding (9).

In HIV, Gag is synthesized in the cytoplasm, migrates to the cellular periphery, and eventually targets the surface of the PM, where the assembly of immature virus occurs (10). As in other retroviral genera, the MA domain of HIV-1 Gag is the structural motif that mediates targeting to the PM (11) where lateral assembly of the viral shell occurs. Distinct molecular signals complement each other in positioning the protein in an orientation productive for assembly on the correct target membrane (12): electrostatic interactions between the basic patch of residues on the globular head and anionic membrane lipids, hydrophobic interaction between MA's myristoylated N terminus and the membrane, and specific binding of the protein to phosphatidylinositol-4,5-bisphosphate [PI(4,5)P₂] (13), a low-abundance phospholipid found principally in the cytoplasmic leaflet of the PM (14). Lipidomic studies show that raft-related lipids, such as sphingomyelin and cholesterol, are enriched in the HIV-1 envelope (15–18). This is consistent with the hypothesis that HIV-1 assembles on microdomains in the PM, possibly lipid rafts, with specific lipid compositions (19–21). Moreover, virion membranes budded from macrophages and from T cells, two distinct preferential tar-

gets of HIV (22, 23), show similar membrane compositions (15) even though the global compositions of macrophage and T-cell membranes are different. This suggests that HIV-1 recruits specific membrane components and thus creates a favorable lipidic environment for its assembly (23).

The binding of HIV-1 MA to bilayer membranes has already been extensively studied (8, 24, 25). MA interactions with PI(4,5)P₂ not only direct Gag assembly to specific regions of the PM but may also help trigger myristate exposure from its sequestered state within the protein (26). Entropic effects may contribute, since it has been reported that myristate exposure favors MA trimerization (27, 28). Moreover, some evidence suggests that the unsaturated chain of PI(4,5)P₂ binds MA upon myristate membrane insertion (26, 28), which would enhance Gag affinity to lipid rafts. On the other hand, important questions remain poorly understood. For example, a clear delineation of how individual bilayer components contribute to MA binding has not yet been achieved, and in particular the impact of protein myristoylation on protein-membrane interactions has not been quantitatively assessed.

In this study, we use surface plasmon resonance (SPR) spectroscopy on synthetic solid-supported bilayers, referred to as sparsely tethered bilayer lipid membranes (stBLMs), to parse protein-membrane interactions into their components. In combination, SPR performed on stBLMs offers unique advantages for the study of viral assembly processes on membranes. Both the stBLM model system (29) and the SPR method for studying intermolecular interactions (30) are well established. SPR offers information not only on the affinity of a ligand to its target surface but also on the equilibrium load of the ligand at that surface (30), i.e., the protein density on the membrane surface. The stBLM platform

(Fig. 1) incorporates a single lipidic bilayer membrane of well-controlled composition that is tethered to a planar electrode—a 0.05- μm -thick Au film on a glass or Si substrate—via short ethyleneoxide anchors (31), thereby providing a hydrated environment on both sides of the membrane. Thereby, the bilayer retains its intrinsic fluidity (32), is virtually defect-free (29), and is resilient to external manipulations such as buffer exchanges, as monitored by electrochemical impedance spectroscopy (33). Its lipidic composition can be precisely controlled (34) and, in particular, functionally important lipids such as PI(4,5) P_2 can be incorporated into the membrane. This may be important, since binding studies that use soluble short-chain PI(4,5) P_2 tend to underestimate binding (26). On the other hand, the low defect density of stBLMs suppresses inflated readings in SPR assays that can occur when protein adsorbs to membrane defects (32). Here, we used dioleoylglycerophosphocholine (DOPC), instead of the more physiologically relevant palmitoyl-oleoyl-PC (POPC), as a background component for bilayers because it forms membranes of higher quality more consistently than POPC. Similarly, we conducted our studies generally at 25°C and in buffers that contain 50 mM salt (NaCl), instead of a more physiologically relevant 150 mM ionic strength, because the MA protein, in particular in its myristoylated form, showed a tendency for aggregation that we were able to avoid under the stated conditions.

Using SPR on stBLMs, we assess the specific roles of electrostatic, hydrophobic, and lipid-specific contributions to viral assembly at the membrane surface. The impact of lipidation is evaluated in a quantitative comparison of the binding of non-myristoylated (–myr) and myristoylated (+myr) protein to such model membranes, and the role of cholesterol (chol) in promoting protein affinity to the bilayer is assessed. Our results show clearly that MA binds the membrane through a combination of specific and nonspecific interactions. We determine the hydrophobic and electrostatic free energies in the nonspecific protein binding to charged membranes and show that these contributions are not simply additive in the total free energy.

MATERIALS AND METHODS

Protein expression and purification. Standard laboratory chemicals, culture media, 1-tridecanecarboxylic acid (myristic acid), isopropyl- β -D-thiogalactopyranoside (IPTG), phenylmethylsulfonyl fluoride (PMSF), β -mercaptoethanol (β -ME), and tris(2-carboxyethyl)phosphine hydrochloride (TCEP) were purchased from Sigma Chemical (St. Louis, MO). Protease inhibitor cocktail set I-Calbiochem was from EMD Millipore (Billerica, MA). Talon metal affinity resin was from Clontech Laboratories, Inc. (Mountain View, CA). SDS-PAGE supplies were from Bio-Rad (Hercules, CA). Columns for protein purification were from GE Healthcare Life Sciences.

MA proteins were expressed in BL21(DE3)/pLysS cells transfected with the PET 3XC vector. For the production of –myrMA, cells were induced at 37°C for 4 h with 1 mM IPTG and lysed in buffer A (20 mM Tris HCl [pH 7.4], 10 mM β -ME, 1 mM PMSF) with 150 mM NaCl. After centrifugation at 12,000 $\times g$ for 15 min to remove cellular debris, the protein was fractionated from the lysate by taking a 40 to 70% ammonium sulfate saturation cut. The protein was dialyzed against buffer A with 150 mM NaCl. Ammonium sulfate was added to 40% saturation, and the solution was chromatographed on a butyl-Sepharose column. Fractions containing the protein were dialyzed against buffer A with 50 mM NaCl and chromatographed on an SP Sepharose column. The purified protein was stored in buffer A with 150 mM NaCl and 10% glycerol and then chromatographed on a Superdex-75 gel filtration column before use.

The plasmid used for the +myrMA preparation via coexpression of

MA protein and *N*-myristoyltransferase (28) was kindly provided by Michael Summers (University of Maryland, Baltimore). For the expression, cells were grown to an optical density at 600 nm (OD_{600}) of 0.4 with shaking (250 rpm) at 37°C and then supplemented with myristic acid at a concentration of 10 mg/liter and kept growing to an OD_{600} of 0.8. At this point, protein expression was induced by adding IPTG to a concentration of 1 mM, and the cells were cultivated at 30°C overnight. Cells were harvested by centrifugation at 6,000 $\times g$ for 15 min at 4°C, washed with PBS, and held frozen at –80°C. Portions (5 g [wet weight]) of cells were resuspended in 30 ml of lysis buffer B (20 mM Tris, 300 mM NaCl, 10% glycerol, 1 mM PMSF, 1 \times protease inhibitor mixture set I-Calbiochem, 1 mM TCEP [pH 7.4]) and disrupted on ice by sonication. The cell lysate was centrifuged at 10,000 $\times g$ for 30 min at 4°C, and the protein was purified by immobilized metal affinity chromatography using the Talon metal affinity resin. Monomeric MA was separated by size exclusion chromatography on a Superdex-75 10/30 GL column using an AKTA purifier system (Amersham Pharmacia Biotechnology).

Lipids and liposome preparation. 1,2-Dioleoyl-*sn*-glycero-3-phosphocholine (DOPC), 1,2-dioleoyl-*sn*-glycero-3-phospho-L-serine (DOPS), cholesterol (extracted from ovine wool), L- α -phosphatidylinositol-4,5-bisphosphate [brain extract; PI(4,5) P_2], and L- α -phosphatidylinositol (soy extract; soy-PI) were obtained from Avanti Polar Lipids. The tether compound HC18 [Z20-(Z-octadec-9-enyloxy)-3,6,9,12,15,18,22-heptaotetracont-31-ene-1-thiol] was synthesized and characterized as described elsewhere (31). Lipid mixtures at the desired molar ratios were prepared from fresh lipid stock in chloroform, and the solvent was evaporated under vacuum for 12 h. The dried lipid films were hydrated in a high-salt aqueous buffer (1 M NaCl, 10 mM NaPO_4 [pH 7.4]) to a lipid concentration of ~ 5 mg/ml and subsequently sonicated until clear lipid solutions were obtained. These were extruded through polycarbonate membranes (100-nm pore size) at least 21 times to obtain uniform distributions of unilamellar liposomes.

Preparation of sparsely tethered bilayer lipid membranes. Microscopy glass slides (1 by 3 in.) were cleaned with sulfuric acid plus Nochromix (Godax Laboratories, Cabin John, MD), followed by rinses with ultrapure water (EMD Millipore) and pure ethanol (Pharmco-Aaper), and then dried in a nitrogen flow. The substrates were loaded into a magnetron (ATC Orion; AJA International) and coated with an ~ 2 -nm Cr adhesion layer, followed by an ~ 45 -nm Au layer. Self-assembled monolayers (SAMs) were prepared by overnight incubation of the Au-coated substrates in 0.2 mM ethanolic solution (total concentration) of HC18 and β -ME in molar ratios of 3:7. Vesicle solutions were then allowed to incubate the SAM-covered slides for at least 2 h, followed by immersion into a low-ionic-strength buffer (50 mM NaCl, 10 mM NaPO_4 [pH 7.4]) that completed stBLM formation (29, 33).

Surface plasmon resonance. SPR measurements were conducted at 25°C \pm 0.01°C in a single-batch set-up using a custom-built instrument (SPR Biosystems, Germantown). SAM-covered, gold-coated glass slides were assembled in the Kretschmann configuration by index-matching to a prism. stBLMs were then completed by vesicle fusion *in situ*, as described above. The setup allows for simultaneous SPR and electrochemical impedance spectroscopy measurements, which were used to assess the quality of the stBLMs before protein was introduced. The light intensity reflected from the glass-buffer interface that carried the membrane was recorded on a two-dimensional charge-coupled device array and the position of the intensity minimum was recorded as a function of time. In the single-batch experiments, the neat bilayer was measured first to determine a baseline before adding protein in increasing concentrations and allowing it to incubate the stBLM. SPR Aria (SPR Biosystems) was used for real-time recording of the light reflection minimum position, R , on the detector and time courses of R were recorded for each protein concentration, c_p , until equilibrated at R_{eq} . The R_{eq} was fitted to the Langmuir isotherm to determine the protein affinity in terms of the dissociation constant (K_d) and the surface density of bound protein (R_{∞}) (30):

$$R_{\text{eq}}(c_p) = \frac{R_{\infty} \cdot c_p}{c_p + K_d} \quad (1)$$

For a case in which the Langmuir isotherm was clearly not a good model to describe the experimental data, we used the Hill equation:

$$R_{\text{eq}}(c_p) = R_{\infty} \cdot \frac{c_p^N}{c_p^N + K_d} \quad (2)$$

Quantification of low protein affinities required high protein concentrations in the buffer. If in excess of 25 $\mu\text{mol/liter}$, protein dissolved in the buffer increases the optical index (n) of the medium in contact with the sensor surface significantly, thus raising the readout. The measurements were corrected for bulk protein effects as follows. The refractive index increment $dn/dc \approx 0.185 \text{ ml/g}$ (35, 36). The sensitivity of the instrument is $\Delta n = (6.4 \pm 0.3) \times 10^{-5}/\text{RU}$, where the response unit (RU) is the shift in the SPR reflection minimum on the detector in pixels (37). The SPR responses at high c_p were accordingly corrected. From a calibration of the SPR instrument (37), we estimate that a densely packed monolayer of MA protein corresponds to an instrument response of $R_{\infty} \approx 58$ pixels, as determined from its molecular cross section ($A = 786 \text{ \AA}^2$), assessed from the nuclear magnetic resonance (NMR) structure (26), in the membrane-bound orientation (38) and the molecular weight. Free binding energies (ΔG) were then calculated from the K_d value:

$$\Delta G = RT \cdot \ln(K_d/c_{\text{ref}}) \quad (3)$$

where c_{ref} is an arbitrary reference concentration, taken here to be 55 M, the concentration of the solvent (39).

RESULTS

The association of Gag with the PM of the host is a complex process in terms of molecular interactions that drive it and lead to the formation of the Gag lattice on the viral membrane in the immature virus. Multiple signals contribute to this process, and here we try to disentangle those signals that relate to the MA domain: electrostatic interaction of MA's cationic patch with acidic membranes, hydrophobic interaction of the myristate with the bilayer, and specific interactions with the PM lipid PI(4,5)P₂ (13). In this approach, we deliberately exclude the role of homotypic protein-protein interactions. In particular, interactions between the Gag CA and sp1 regions are known to promote oligomerization, which can greatly enhance Gag membrane targeting and induce cooperativity in Gag membrane binding, as recently shown for RSV Gag (9), whereas binding of the NC domain to nucleic acids is presumably cooperative, thus indirectly promoting association between Gag molecules.

By varying membrane compositions in stBLMs (Fig. 1) and quantifying the affinities of nonmyristoylated and myristoylated MA protein at a standardized buffer composition (50 mM NaCl, 10 mM NaPO₄ [pH 7.4]) by SPR, this study seeks to disentangle the contributions of the physical interactions that lead to MA membrane binding. The lipid compositions were chosen to resemble the major lipid components of the locus at which viral assembly is initiated, i.e., the inner leaflet of the plasma membrane (PM). However, because phosphatidylethanolamine (PE) at high concentrations does not form stable bilayers in stBLMs, we used DOPC, which forms high-quality bilayers more consistently than the physiologically more relevant POPC, as the majority component of the bilayers. In this backdrop of DOPC, we investigated the role of DOPS, cholesterol (chol), and PI(4,5)P₂. In order to characterize the impact of the myristate group and lipid composition on the HIV-1 MA-membrane association, we systematically stud-

ied the interactions of $-myrMA$ and $+myrMA$ with multicomponent stBLMs.

Myristoylation increases the MA membrane affinity by over an order of magnitude on PS-containing stBLMs. MA binding to pure DOPC stBLMs was below the detection limit for both $-myrMA$ and $+myrMA$. However, both proteins bound readily to PS at concentrations of 10 mol% and higher in the bilayer, as shown by the binding isotherms in Fig. 2. As observed earlier (38), electrostatic interactions alone were sufficient to attract $-myrMA$ to the membrane surface (Fig. 2A), and variations in PS concentration led to significant differences both in affinity (K_d) and protein load (R_{∞}), i.e., the in-plane density of protein bound to the membrane (equation 1). At high PS concentrations (>40 mol%), the protein load approached levels expected for a densely packed protein monolayer ($R_{\infty} \approx 60$), albeit with low affinities. Even for a stBLM composed of 100% PS, K_d did not fall below 10 μM . Lipidated $+myrMA$ showed consistently higher affinities to DOPS-containing stBLMs (Fig. 2B) and was more sensitive to PS concentration in the bilayer. While the protein load of the membrane was similar for $+myrMA$ and $-myrMA$ (Fig. 2D), affinities of $+myrMA$ were about an order of magnitude larger than those of $-myrMA$, resulting in free energy differences, $\Delta\Delta G \approx 5$ to 8 kJ/mol, as shown in Fig. 2C. A summary of these results is compiled in Table 1.

The dependence of protein surface density on PS concentration was described by a simple model based on the probability that MA encounters a certain number of anionic PS molecules underneath its projection on the membrane. Assuming that this number of electrostatic contacts is required for stably binding the protein to the membrane and that lipid diffusion is negligible, this probability is proportional to the experimentally observed protein load on the membrane, R_{∞} . Even though oversimplified, this model describes the increase of protein surface density at different PS concentrations in the membrane surprisingly well (Fig. 2D), predicting that three PS lipids interact directly with each MA in ligating the protein to the surface. The model also predicted that the MA footprint covers ~ 12 lipids in the membrane, in agreement with straightforward calculations based on MA cross section (26) and the area per lipid ($\sim 70 \text{ \AA}^2$ per molecule).

The results presented here show that myristoylation makes a substantial contribution to MA membrane binding, as expected, even if the remaining interactions were reduced to the electrostatic attraction. The strength of our experimental approach—the quantitative assessment of protein affinity to the membrane and protein accumulation at its surface—affords a direct determination of free-energy changes (Fig. 2C) and an estimate of the stoichiometry of interactions (Fig. 2D). Thereby, the results in Fig. 2 serve as a backdrop for investigations of membranes of progressively higher complexity.

Cholesterol affects $+myrMA$ targeting to charged membranes. Cholesterol by itself is a bilayer component that does not engage directly in interactions between Gag and the membrane. However, it has been demonstrated to affect Gag membrane binding strongly (40). To understand this apparent contradiction, we note that cholesterol influences the physical properties of membranes and their organization (41), most prominently in terms of the formation of cholesterol-enriched membrane microdomains (42, 43), and these changes are likely to affect Gag binding (20). To investigate the impact of cholesterol on MA membrane binding quantitatively, various amounts of cholesterol were introduced

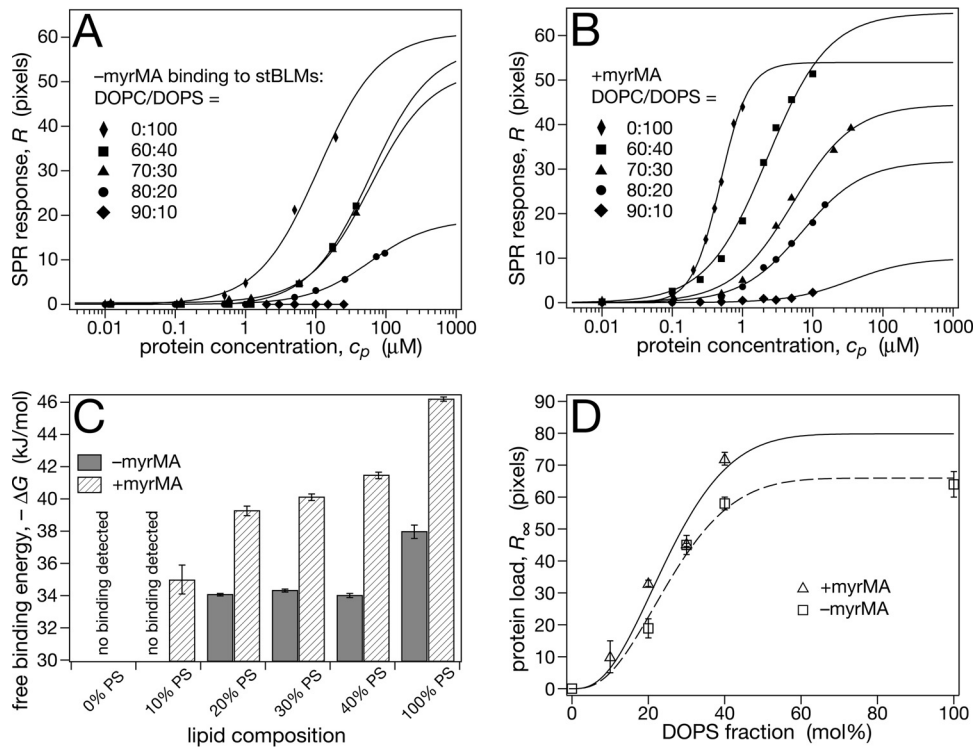


FIG 2 Comparison of $-myrMA$ and $+myrMA$ binding to stBLMs that contain DOPC and DOPS. The buffer consisted of 10 mM Na_2PO_4 and 50 mM NaCl (pH 7.4). (A) Representative SPR curves of $-myrMA$ binding, analyzed with the Langmuir model (equation 1). (B) Representative SPR curves for $+myrMA$. Binding to 100% DOPS stBLMs showed significant deviations from a Langmuir isotherm and was analyzed with the Hill model (equation 2), yielding a Hill coefficient of $n \approx 2$. (C) Free binding energies, ΔG (equation 3), derived from the data shown in panels A and B. (D) Saturation protein surface densities, R_∞ . Lines are guides to the eye, indicating saturation of the equilibrium protein load for stBLMs containing more than ~ 40 mol% DOPS. The R_∞ value for $+myrMA$ binding to a 100% DOPS stBLM is excluded from the plot, since it was determined using a different binding model. Measurements were performed at least in triplicate; error bars in panels C and D indicate standard mean deviations from the average. For low-affinity isotherms, it was not possible to measure full binding curves due to limitations in available amounts of protein.

into DOPC stBLMs with a constant amount of DOPS. The results in Fig. 3A show no significant change in affinity of $-myrMA$ compared to cholesterol-free stBLMs. For $+myrMA$, Fig. 3B, cholesterol increased the membrane affinity by a factor of ~ 2.5 , without significant differences for cholesterol concentrations between 10 and 30 mol%.

The protein load at saturation increased for both proteins, and in particular the membrane load of $+myrMA$ almost doubled in the presence of cholesterol in DOPC/DOPS membranes.

These results show that cholesterol by itself does not contribute to MA affinity for membranes that attract the protein through

TABLE 1 Best-fit parameters obtained from the Langmuir model, equation 1, for data shown in Fig. 1, 2, 3, and 5^a

Membrane composition (ratio)	Mean \pm SEM			
	$-myrMA$		$+myrMA$	
	K_d (μM)	R_∞ (pixels)	K_d (μM)	R_∞ (pixels)
100% DOPC	NB	NB	NB	NB
DOPC:DOPS (90:10)	NB	NB	40 ± 15	10 ± 5
DOPC:DOPS (80:20)	57 ± 2	18.9 ± 0.8	7.0 ± 0.9	33 ± 1
DOPC:DOPS (70:30)	52 ± 2	45 ± 3	5.0 ± 0.4	45 ± 0.5
DOPC:DOPS (60:40)	59 ± 3	58 ± 2	2.9 ± 0.2	72 ± 2
100% DOPS	12 ± 2	64 ± 4	0.5 ± 0.1	54 ± 1^b
DOPC:DOPS:chol (40:30:30)	48 ± 3	68 ± 1	2.1 ± 0.1	84 ± 0.6
DOPC:PI(4,5)P ₂ (95:5)	6.7 ± 0.4	22.3 ± 0.7	1.8 ± 0.2	35 ± 0.3
DOPC:DOPS:PI(4,5)P ₂ (80:15:5)	8.2 ± 0.7	25.9 ± 0.7	1.4 ± 0.1	58 ± 2
DOPC:DOPS:PI(4,5)P ₂ :chol (50:15:5:30)	2.1 ± 0.1	44 ± 0.7	0.8 ± 0.1	80 ± 5
DOPC:PI (70:30)	ND	ND	11.5 ± 0.9	39 ± 1
DOPC:PI:PI(4,5)P ₂ (80:15:5)	ND	ND	2.4 ± 0.2	20 ± 1

^a NB, no binding detected; ND, not determined.

^b Fitted to the Hill model (equation 2) ($n = 2$).

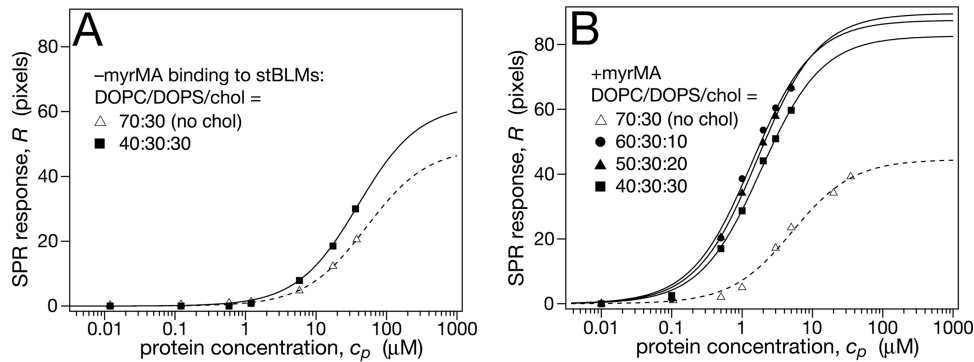


FIG 3 Effect of membrane-bound cholesterol on MA binding to stBLMs containing DOPC and DOPS. The buffer consisted of 10 mM Na_2PO_4 and 50 mM NaCl (pH 7.4). (A) $-myrMA$ adsorption isotherm at 30 mol% cholesterol. (B) $+myrMA$ adsorption isotherms at various cholesterol concentrations between 10 and 30 mol%.

electrostatic interactions. Neither unmyristoylated nor myristoylated MA shows significant changes in affinity. However, the $+myrMA$ accumulation at the membrane surface is affected, which suggests that cholesterol facilitates membrane insertion of the myristate, although it does not increase the gain in free energy associated with insertion.

Cholesterol and PI(4,5) P_2 enhance MA membrane affinity cooperatively. PI(4,5) P_2 is the major PIP lipid in the plasma membrane that distinguishes the mammalian PM, as viewed from the cytosol, from internal membranes (14), and HIV Gag has a well-defined binding pocket for this phosphatidylinositide in its MA domain (26). It is therefore generally assumed that PI(4,5) P_2 provides the main signal that directs HIV Gag to the PM as the locus of productive assembly, and indeed, perturbation of cellular PI(4,5) P_2 interferes with proper Gag assembly (13, 15, 44). However, quantitative data that characterize the binding of HIV-1 MA to PI(4,5) P_2 are scarce, in particular for $+myrMA$. We therefore investigated protein binding to PI(4,5) P_2 -containing membranes, specifically in the context of the other membrane components discussed above. Figure 4 reports the interaction of MA with membranes that contained PI(4,5) P_2 . For DOPC with PI(4,5) P_2 only, the membrane affinity of $-myrMA$ increased almost by a factor of 10 over that observed on a bilayer that contained DOPS at a similar surface charge density. Because the PI(4,5) P_2 headgroup

bears a charge of -4 at neutral pH (45), membranes that contain 20 mol% DOPS, shown as references in Fig. 4, can be compared in their electrostatic interaction to the protein with membranes that contain 5% PI(4,5) P_2 . For $+myrMA$, the increase was more than a factor of 3. The protein coverage remained about the same in both situations. The addition of PS to a PI(4,5) P_2 -containing membrane had no effect on $-myrMA$ membrane binding (Fig. 4A) and resulted in an increase of the protein load, but not affinity, for $+myrMA$ (Fig. 4B). On this background, the addition of cholesterol made a substantial difference in protein binding. Membrane affinities increased only moderately, by factors of ~ 4 and ~ 2 , respectively, for $-myrMA$ and $+myrMA$, but the impact on the protein load was pronounced in both cases. In particular in the binding of $-myrMA$, cholesterol showed a significant cooperativity with PS and PI(4,5) P_2 in attracting the protein to the membrane surface. This effect was weaker for $+myrMA$. Figure 5 summarizes the results on MA membrane binding to cholesterol and PI(4,5) P_2 -containing membranes in terms of free energies of binding, ΔG .

The results reported here for PI(4,5) P_2 -containing membranes and membranes that contained both the phosphatidylinositide and cholesterol showed convincingly that there is a pronounced synergy between the two membrane components. Neither PI(4,5) P_2 nor cholesterol by itself increased HIV MA membrane

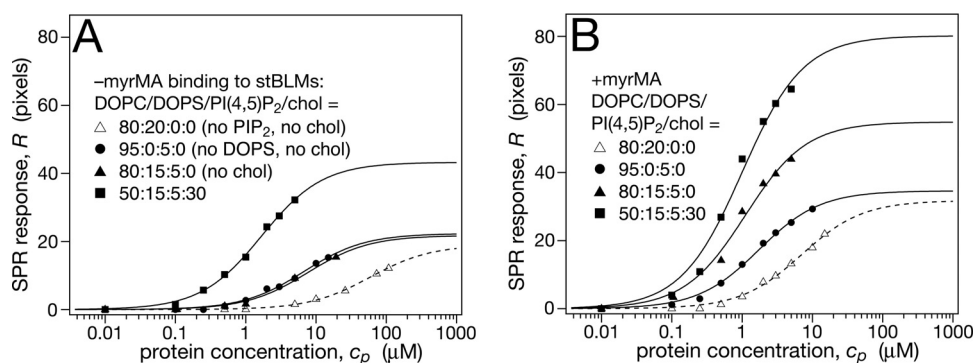


FIG 4 Effect of membrane-bound cholesterol on MA binding to stBLMs containing DOPC, DOPS and PI(4,5) P_2 . The buffer consisted of 10 mM Na_2PO_4 and 50 mM NaCl (pH 7.4). (A and B) $-myrMA$ adsorption isotherms (A) and $+myrMA$ adsorption isotherms (B) at 15 mol% DOPS and 5 mol% PI(4,5) P_2 in the absence or presence of cholesterol. To visualize the effect of PI(4,5) P_2 specificity in binding DOPC/DOPS (80:20; same data as in Fig. 2A and B) is shown for a reference. Because the PI(4,5) P_2 headgroup has ~ 4 anionic charges at neutral pH (45), the charge density of the DOPC/DOPS and DOPC/PI(4,5) P_2 stBLMs is comparable.

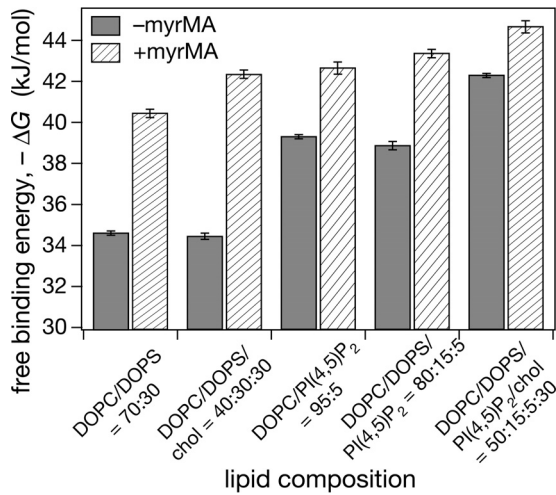


FIG 5 Free binding energies, ΔG , of MA to stBLMs derived from the data shown in Fig. 3 and 4. DOPC/DOPS (70:30; same data as in Fig. 2C) is shown for a reference. Measurements were performed at least in triplicate, with mean deviations shown as error bars.

binding notably, but in combination they boosted both binding affinity, i.e., free energy gained from binding, and protein accumulation at the surface. The aggregate of results reported in Fig. 2C and 5 and Table 1 show that the difference in ΔG for membrane binding of +myrMA between a complex bilayer that contained DOPC, DOPS, PI(4,5)P₂, and cholesterol and a binary DOPC/DOPS bilayer that contained charged lipid in physiological concentration ($\sim 10\%$) is about 10 kJ/mol, a significant fraction of the strength of a covalent bond. Neither of the physical interactions measured separately came close to this result by itself, and cholesterol was apparently required to merge the individual contributions into an aggregate interaction that showed the high binding avidity that we measured for the complex membrane.

+myrMA binds preferentially to PS-containing, but not to PI-containing membranes. Phosphatidylinositol (PI) is the second most concentrated acidic component of the inner PM after PS and, in contrast to PS, is underrepresented in the viral shell, where it only appears in trace amounts (16). However, because PI has the same charge as PS, it provides a control to determine whether the modest enrichment of PS in the viral shell (18) is entirely of electrostatic origin. Alternatively, this interaction may include some element of specificity, either with the protein or with the environment of PS in the cell membrane which could lead to its enrichment through cosorting with raft-related lipids. If the latter was true, one would expect that the affinity of MA to PI-containing membranes is similar to that observed for PS-containing membranes. Our results show that this is indeed the case: the affinity of +myrMA to PI-containing stBLMs was only slightly lower, by $\sim 50\%$, than that observed for DOPC/DOPS membranes of equivalent composition, and the protein load was only marginally reduced (compare data in Fig. 2A and 4A to Fig. 6). For stBLMs that contained PI(4,5)P₂ in addition to PI, we observed a larger reduction in protein load after substituting PS with PI, but the membrane affinity of the protein was also roughly equal for both monovalent lipids. With the caveat that chain composition of membrane lipids also affects Gag protein binding (40, 46) and that they differed between the PS and PI in our experiments, these

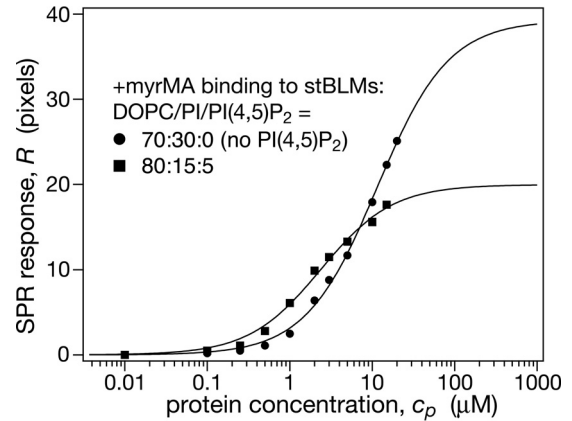


FIG 6 SPR binding curves of +myrMA to DOPC stBLMs containing DOPC and PI with or without PI(4,5)P₂ at approximately equivalent surface charge densities of the membranes. The buffer consisted of 10 mM Na₂PO₄ and 50 mM NaCl (pH 7.4).

results are nevertheless consistent with the hypothesis that PS is preferentially sorted into the viral shell, albeit at a moderate level. This control experiment thus indicates that electrostatic interactions of the MA protein are similar with PS and PI and suggests that differential mixing of the lipids into the domain structure within the biological membrane, rather than differing physical interactions, are responsible for their distinct enrichment characteristics in the assembled viral protein/membrane shell.

DISCUSSION

The HIV-1 MA protein is that domain of the Gag polyprotein which interacts with the membrane that encloses the assembled, immature virus particle. Since this membrane envelope is acquired from the plasma membrane of the host cell during budding, it contains lipids and proteins found in the PM (47, 48). In this context, it is well known that specific lipids, in particular cholesterol, phosphatidylserine, and sphingomyelins, are enriched in the viral membrane envelope, whereas PC and PI are under-represented, resulting in the unique composition of the viral lipidome (15–18). In cells, myristoylation of Gag is a prerequisite for plasma membrane targeting (49–52), since mutation of the N-terminal glycine completely blocks membrane localization of Gag and the subsequent assembly of infectious virus particles (53). Although the Gag nucleocapsid (NC) domain can compete with MA for association with the acidic surface of the inner PM, thus ligating Gag to the membrane surface in a U-shaped conformation (54), it dissociates the lipid upon exposure to nucleic acid (55). The membrane-bound polyprotein thus assumes an extended conformation on the bilayer surface that promotes lateral interactions between the capsid domains, leading to the formation of the two-dimensional protein lattice that defines the immature capsid (10, 56). A decisive step in this supramolecular self-assembly process that is determined by the atomistic details of the protein-membrane interface of the viral shell is thus the interaction of MA with the inner PM surface.

Although our experiments were performed at 25°C due to experimental limitations, whereas previous NMR studies were done at the physiologically more relevant temperature of 35°C (26, 28), this might not be the only explanation for the discrepancy of our results with these publications. In insect cells grown at 28°C, ex-

pression of Gag results in formation of VLPs at the PM, which depends strictly on the myristoylation of Gag (57). Therefore, the importance of the myristate in Gag targeting is temperature invariant, at least as judged from this singular example. In addition, since myristoylation of MA leads to its multimerization, and this association is more pronounced in MA-CA constructs, the influence of PI(4,5)P₂ on membrane binding may be more pronounced on longer Gag constructs that promote protein-protein interaction between its domains. Moreover, the monomer-trimer equilibrium for +myrMA is temperature dependent (see the caption to Fig. 1 in reference 28). A study reported the influence of PI(4,5)P₂ on Gag membrane binding (58) at 30°C (incubation), but the flotation was performed at 4°C. Besides using full-length Gag (as opposed to the MA domain in our study), these experiments also contained a host of proteins from the reticulocyte lysate. Another flotation study of HIV Gag reported that PI(4,5)P₂ or PS enhances liposome binding to similar extent (59).

Roles of membrane charge and protein lipidation. Binding of –myrMA to PS-containing membranes is enabled by electrostatic interactions between the charges on the protein and the anionic membrane (38). A cationic patch on the surface of MA formed by Arg4, Lys26, Lys27, Lys30, Lys32, and Arg39 was shown by neutron reflection to dive into the surface of the anionic bilayer at a distance where it can directly interact with membrane headgroups (38). Protein myristoylation adds a hydrophobic component to the interaction, since the myristate can insert into the hydrocarbon core of the membrane. However, the myristate increases MA membrane association only moderately in the absence of either cholesterol or PI(4,5)P₂ from the membrane. On pure PC/PS bilayers, MA affinity differed by a factor of ~10 ($\Delta\Delta G \approx 6$ kJ/mol) between the myristoylated and nonmyristoylated proteins, in qualitative agreement with vesicle flotation assays (8). Distinct from flotation assays, we determined dissociation constants with SPR that were two orders of magnitude lower ($K_d \approx 5$ and ≈ 50 μ M, respectively, for +myrMA and –myrMA), a finding consistent with a tendency of flotation assays to underestimate the affinities of protein to liposomes (25).

Although substantial, the observed gain in free binding energy ($\Delta\Delta G \approx 6$ kJ/mol) of +myrMA over –myrMA was smaller than that expected from fully inserting a myristoyl chain from solution into a lipid membrane, which is estimated to yield ≈ 48 kJ/mol (60, 61). Several effects could reduce the free binding energy. (i) Transfer of the myristoyl from its hydrophobic sequestration within the dissolved protein into the bilayer is likely associated with a lower enthalpy change than transfer of a free fatty acid from aqueous solution. (ii) The myristoyl group may only partially insert, as has been previously proposed in a different molecular context (60). (iii) A myristoyl membrane anchor further reduces the bound protein's entropy compared to the nonlipidated species, as recently shown for the membrane-bound, myristoylated GRASP domain (62).

While the gain in binding energy conferred by the myristate on PI(4,5)P₂-free membranes was smaller than expected, our results show clearly that MA interaction with PI(4,5)P₂ is not a requirement to trigger myristate exposure at the PM, as previously suggested (26). Indeed, they agree with recent NMR studies which suggested that the myristate is readily exposed on MA bound to bicelles or micelles that lack PI(4,5)P₂ (27). Membrane binding and PM targeting are separable events. Mutations to charged residues in MA, or deletion of residues 84 to 88, cause mistargeting

and assembly to Golgi or post-Golgi vesicles (11). We observed that the gain in free binding energy of –myrMA depends only weakly on the PS content of the membrane, while it increased substantially for +myrMA. Therefore, our results can be interpreted to imply that MA membrane binding does not strictly depend on a lipid-mediated key-and-lock trigger that initiates myristate exposure but that the myristate rather is in a thermodynamic equilibrium between the exposed and sequestered states that may depend on the charge density of the membrane encountered.

Role of PI(4,5)P₂. Although the interaction between MA and PI(4,5)P₂ has already been investigated by a variety of biophysical techniques (26, 58, 63, 64), quantitative binding data of the protein to this lipid in the context of bilayer membranes are still scarce (65) and data measured out of the membrane context tend to underestimate affinities. For example, solution NMR studies reported a dissociation constant (K_d) of ≈ 150 μ M for myristoylated HIV-1 MA with soluble di-C₄-PI(4,5)P₂ and a slightly higher affinity to di-C₈-PI(4,5)P₂ (26). A recent SPR investigation in which tetraphosphorylated inositol (IP₄) was immobilized on the sensor chip and competitive binding with preequilibrated MA/di-C₈-PI(4,5)P₂ was determined, reported a dissociation constant of +myrMA to dissolved di-C₈-PI(4,5)P₂ of $K_d \approx 5$ μ M (64). These earlier results, all performed out of the context of the membrane, thereby indicate affinities that are lower by factors of 3 to 100 than the SPR results reported here, which suggests that the membrane context is essential for obtaining thermodynamic data.

The addition of 5 mol% PI(4,5)P₂ to DOPC stBLMs resulted in binding affinities of –myrMA and +myrMA larger than those to DOPC with 30 mol% DOPS (Table 1). However, assuming an effective charge between $-3e$ and $-4e$ for PI(4,5)P₂ at physiological pH (66), the charge density of a membrane surface containing 5 mol% PI(4,5)P₂ is lower than that brought about by 30 mol% DOPS. The experimental result then shows that PI(4,5)P₂ binding to MA involves more than simple electrostatic interaction. This is not surprising, since it is well established that MA binds to dissolved short-chain PI(4,5)P₂ in a specific manner (26). For both –myrMA and +myrMA, the protein load at saturation on stBLMs that contain 5 mol% PI(4,5)P₂ equaled that on 20 mol% DOPS. When MA bound to a membrane that contained 20 mol% DOPS, ≈ 2.4 DOPS lipids, on average, were within the protein footprint on the bilayer, which in turn is about $12\times$ the area of a lipid molecule (68 to 73 \AA^2) for monounsaturated lipids (67). From the quantification of the protein load on the bilayers, it then follows that the average number of PI(4,5)P₂ molecules bound per MA in the 5 mol% PI(4,5)P₂ stBLM does not exceed two.

When increasing the complexity of the membrane from a binary DOPC/DOPS bilayer to a DOPC/DOPS/PI(4,5)P₂ system, we observed no significant affinity changes for –myrMA and +myrMA compared to 5 mol% PI(4,5)P₂ (Table 1). The protein load at saturation, R_∞ , remained constant for –myrMA and increased only slightly for +myrMA. An interpretation remains difficult due to the lack of a comprehensive PC/PS/PI(4,5)P₂ phase diagram. However, we point out that both –myrMA and +myrMA SPR isotherms on 15 mol% DOPS + 5 mol% PI(4,5)P₂ in DOPC are simple additions of the individual SPR curves on 15 mol% DOPS and 5 mol% PI(4,5)P₂ in the DOPC background. If nothing else, this argues for a lack of cooperative effects between DOPS and PI(4,5)P₂ binding, and it is interesting to speculate that this may result from a lack of mixing of PI(4,5)P₂ and DOPS on

the length scale of the footprint of the MA protein on the bilayer. Our comparative measurements of +myrMA adsorption to bilayers that contained PI instead of PS—with or without PI(4,5)P₂—did not reveal any major differences. This would suggest that PS and PI should be similarly enriched in the viral shell if electrostatic attraction determines lipidomic selection. The fact that PS is moderately over-represented while PI is underrepresented in the viral shell (16, 18), however, may imply that PS preferentially incorporates into cholesterol-rich domains enriched in PI(4,5)P₂, whereas PI does not.

Role of cholesterol. There is no known physical mechanism that promotes direct interactions between membrane-associated Gag and cholesterol. Moreover, neutron reflection studies of HIV Gag on phospholipid membranes showed that the protein associates with the bilayer only peripherally, interacting with the phospholipid headgroups but not the hydrophobic membrane core (38). However, it was also shown that Gag interaction with bilayers is sensitive to the composition of the interior of the bilayer and in particular to the presence of cholesterol (40). In the results presented here, the largest differences between +myrMA and -myrMA binding affinities were observed on bilayers that contained PS and cholesterol (left-hand bars in Fig. 5). These arise because the affinity of -myrMA on DOPC/DOPS stBLMs was insensitive to cholesterol whereas the affinity of +myrMA increased significantly in the presence of cholesterol. For both MA proteins, we also observed a significant increase in the protein load at saturation, by ≈50% for -myrMA and by almost 100% for +myrMA. This shows that the binding of both the myristoylated and unmyristoylated proteins to PS-containing membranes was affected by cholesterol, despite the lack of an affinity change for -myrMA, and points to the hydrocarbon region of the lipid bilayer as the origin of these effects. It is well established that cholesterol condenses fluid bilayers by changing lipid packing (68–71). However, the observed increases in protein density at the membrane were much larger than the cholesterol-induced increase in lipid density. Therefore, different mechanisms must contribute to the observed results.

The cholesterol-driven increase in binding affinity of +myr MA could be aided by a compatibility effect that may help the myristate insert in the hydrophobic membrane core composed of unsaturated oleoyl chains in the stBLMs under study. The sterol backbone of cholesterol is asymmetrically substituted with methyls that emerge on one face of the ring system, denoted α , rendering this face rough on the atomistic scale, whereas the β -face, which lacks such substitutions, is smooth (72, 73). MD simulations suggested substantial impact of this asymmetry on the binding of cholesterol to saturated (α -face) and unsaturated (β -face) lipid chains (72) and the orientation of the sterol backbone within the bilayer (74). In the light of these results, we speculate that cholesterol is essential to mediate insertion of the saturated myristate into the unsaturated DOPC matrix of the bilayer core. Of course, biological membranes do not consist of pure lipid species but rather of complex mixtures of lipidic components that may segregate locally into distinct domains, driven by a tendency of cholesterol to associate preferentially with saturated chains (75). Our results show that the myristoylated MA protein has a predilection to associate with cholesterol-rich membrane regions, and it is likely to help recruit such patches into the viral membrane shell. It has been shown that myristate substitution with an unsaturated analogue blocks Gag association with detergent-resistant

membranes (76), suggesting that the myristate is a key driver for Gag association with lipid rafts. Our results are consistent with this conclusion and explain *in vivo* results which showed that redistribution of cholesterol from the PM to late endosomes causes relocation of assembly (76) and that cholesterol depletion disrupts Gag membrane binding and, eventually, virus release (19, 77).

Although cholesterol does not affect the binding affinity of -myrMA binding to DOPC/DOPS stBLMs, it increased the affinity to membranes that contain DOPC, DOPS and PI(4,5)P₂ significantly. In distinction to PI(4,5)P₂-free membranes, this increase was even larger for -myrMA than for +myrMA (Table 1). In experimental studies of its effects on lipid packing, cholesterol was shown to increase the average headgroup-to-headgroup distance for DOPC-containing membranes (71). Because PC headgroups are bulky and therefore are likely to reduce MA binding to PI(4,5)P₂, it is conceivable that cholesterol facilitates MA access to PI(4,5)P₂ by spacing out the surrounding DOPC headgroups. Moreover, recent MD simulations suggested that MA may induce lateral segregation of PI(4,5)P₂ into domains which may by itself promote efficient MA binding, for example through locally enhanced electrostatic interactions (78). There is also experimental evidence that cholesterol helps stabilize PI(4,5)P₂ in lipid clusters (79), which rationalizes that cholesterol and PI(4,5)P₂ synergistically attract MA to the membrane, as shown in Fig. 4 and 5. Furthermore, our results are consistent with the finding that PI(4,5)P₂ is enriched in the viral envelope in comparison to host cell membranes (15) and compatible with the idea that Gag triggers the formation of PI(4,5)P₂-enriched domains instead of associating with preexisting microdomains (21, 80). Thereby, a coherent understanding of the roles of molecular interactions emerges that is consistent with the hypothesis that Gag membrane binding depends on cholesterol-rich lipid microdomains and triggers local enrichment of its preferred lipidic interaction partners, most notably PI(4,5)P₂, in its membrane-protein shell.

Conclusions. The quantitative binding measurements reported here provide a consolidated picture on how MA interacts with various major components of the PM and the role of its N-terminal lipidation in the overall process. Our comparative study of -myrMA and +myrMA association with well-defined membrane models of progressively higher compositional complexity showed that the various membrane components are cooperative in their interaction with the MA protein, which may explain their selective recruitment into the viral membrane shell. We observed an increase in MA membrane association due to myristoylation in the absence of either cholesterol or PI(4,5)P₂ from the membrane. On pure PC/PS bilayers, MA affinity differed by a factor of 10× between the myristoylated and unmyristoylated protein: $K_d \approx 5 \mu\text{M}$ versus $\approx 50 \mu\text{M}$. In its trend, this result is in agreement with vesicle flotation assays (8). However, our measurements with SPR on stBLMs quantified the affinity with a half-point concentration that is 2 orders of magnitude lower than those observed with flotation assays (8, 25, 81). The observation that myristoylated MA bound substantially better to PI(4,5)P₂-free bilayers than -myrMA suggests further that PI(4,5)P₂ is not required for triggering myristate exposure, as previously concluded (26).

We then observed that cholesterol facilitated the interaction of the myristate with the target membrane and of PI(4,5)P₂ with the protein. Electrostatic attraction and hydrophobic interaction were sufficient to stably anchor MA at the membrane. While elec-

trostatic interactions alone only led to weak binding of –myrMA, even at low ionic strength (50 mM NaCl), myristoylation increased protein affinity to the bilayer, and both cholesterol and PI(4,5)P₂ augmented MA membrane binding significantly. It thus appears that cholesterol promotes access of the protein to the membrane. In the absence of PI(4,5)P₂, cholesterol increased protein affinity to membranes only for the myristoylated protein, consistent with its role to enhance the compatibility of saturated and unsaturated membrane components, as shown in MD simulations (72). In combination, cholesterol and PI(4,5)P₂ increased membrane binding of –myrMA and +myrMA to a similar extent, which indicates that cholesterol particularly facilitates MA access to the phosphatidylinositol headgroup in a way which is independent of the myristate. Further interaction studies, using Gag constructs with multiple domains, Gag MA targeting mutants, without and in the context of nucleic acids, should shed more light on these differences. Overall, the molecular level details reported here provide a better understanding of the lipid interactions of MA and their implications for proper Gag membrane association, lipid recruitment to the viral shell and viral particle assembly.

ACKNOWLEDGMENTS

We thank D. Worcester and S. Tristram-Nagle for insightful discussions.

This study was supported by the National Institutes of Health (NIH) through grant R01GM101647 (to M.L.), by the Intramural Research Program of the NIH, National Cancer Institute, Center for Cancer Research, and by a grant from the Intramural AIDS Targeted Antiviral Program of the National Cancer Institute, Center for Cancer Research (to A.R.).

H.N., M.L., S.A.K.D., and A.R. designed the research. S.A.K.D. and I.K. purified and characterized the proteins. H.N., M.B., and M.L. planned the experiments, which were conducted by M.B. and evaluated by M.B. and F.H. All authors discussed the results and commented on the manuscript at all stages.

FUNDING INFORMATION

This work, including the efforts of Alan Rein, was funded by HHS | NIH | National Cancer Institute (NCI). This work, including the efforts of Marilia Barros and Mathias Lösche, was funded by HHS | NIH | National Institute of General Medical Sciences (NIGMS) (R01GM101647).

REFERENCES

- Coffin JM, Hughes HH, Varmus HE (ed). 1997. *Retroviruses*. Cold Spring Harbor Laboratory Press, Plainview, NY.
- Hill CP, Worthylake D, Bancroft DP, Christensen AM, Sundquist WI. 1996. Crystal structures of the trimeric human immunodeficiency virus type 1 matrix protein: implications for membrane association and assembly. *Proc Natl Acad Sci U S A* 93:3099–3104. <http://dx.doi.org/10.1073/pnas.93.7.3099>.
- Murray PS, Li Z, Wang J, Tang CL, Honig B, Murray D. 2005. Retroviral matrix domains share electrostatic homology: models for membrane binding function throughout the viral life cycle. *Structure* 13: 1521–1531. <http://dx.doi.org/10.1016/j.str.2005.07.010>.
- Zhou WJ, Parent LJ, Wills JW, Resh MD. 1994. Identification of a membrane binding domain within the amino-terminal region of human immunodeficiency virus type 1 Gag protein which interacts with acidic phospholipids. *J Virol* 68:2556–2569.
- Resh MD. 1999. Fatty acylation of proteins: new insights into membrane targeting of myristoylated and palmitoylated proteins. *Biochim Biophys Acta* 1451:1–16. [http://dx.doi.org/10.1016/S0167-4889\(99\)00075-0](http://dx.doi.org/10.1016/S0167-4889(99)00075-0).
- Gamble TR, Yoo S, Vajdos FF, von Schwedler UK, Worthylake DK, Wang H, McCutcheon JP, Sundquist WI, Hill CP. 1997. Structure of the carboxyl-terminal dimerization domain of the HIV-1 capsid protein. *Science* 278:849–853. <http://dx.doi.org/10.1126/science.278.5339.849>.
- Datta SAK, Zhao Z, Clark PK, Tarasov S, Alexandratos JN, Campbell SJ, Kvaratskhelia M, Lebowitz J, Rein A. 2007. Interactions between HIV-1 Gag molecules in solution: an inositol phosphate-mediated switch. *J Mol Biol* 365:799–811. <http://dx.doi.org/10.1016/j.jmb.2006.10.072>.
- Dalton AK, Ako-Adjei D, Murray PS, Murray D, Vogt VM. 2007. Electrostatic interactions drive membrane association of the human immunodeficiency virus type 1 Gag MA domain. *J Virol* 81:6434–6445. <http://dx.doi.org/10.1128/JVI.02757-06>.
- Dick RA, Barros M, Jin D, Lösche M, Vogt VM. 2016. Membrane binding of the Rous sarcoma virus Gag protein is cooperative and dependent on the SPA domain. *J Virol* 90:2473–2485. <http://dx.doi.org/10.1128/JVI.02733-15>.
- Sundquist WI, Kräusslich H-G. 2012. HIV-1 assembly, budding, and maturation. *Cold Spring Harb Perspect Med* 2:a006924. <http://dx.doi.org/10.1101/cshperspect.a006924>.
- Ono A, Orenstein JM, Freed EO. 2000. Role of the Gag matrix domain in targeting human immunodeficiency virus type 1 assembly. *J Virol* 74: 2855–2866. <http://dx.doi.org/10.1128/JVI.74.6.2855-2866.2000>.
- Bell NM, Lever AML. 2013. HIV Gag polyprotein: processing and early viral particle assembly. *Trends Microbiol* 21:136–144. <http://dx.doi.org/10.1016/j.tim.2012.11.006>.
- Ono A, Ablan SD, Lockett SJ, Nagashima K, Freed EO. 2004. Phosphatidylinositol-(4,5)-bisphosphate regulates HIV-1 Gag targeting to the plasma membrane. *Proc Natl Acad Sci U S A* 101:14889–14894. <http://dx.doi.org/10.1073/pnas.0405596101>.
- van Meer G, Voelker DR, Feigenson GW. 2008. Membrane lipids: where they are and how they behave. *Nat Rev Mol Cell Biol* 9:112–124. <http://dx.doi.org/10.1038/nrm2330>.
- Chan R, Uchil PD, Jin J, Shui G, Ott DE, Mothes W, Wenk MR. 2008. Retroviruses human immunodeficiency virus and murine leukemia virus are enriched in phosphoinositides. *J Virol* 82:11228–11238. <http://dx.doi.org/10.1128/JVI.00981-08>.
- Aloia RC, Tian H, Jensen FC. 1993. Lipid composition and fluidity of the human immunodeficiency virus envelope and host cell plasma membranes. *Proc Natl Acad Sci U S A* 90:5181–5185. <http://dx.doi.org/10.1073/pnas.90.11.5181>.
- Brügger B, Glass B, Haberkant P, Leibrecht I, Wieland FT, Kräusslich H-G. 2006. The HIV lipidome: a raft with an unusual composition. *Proc Natl Acad Sci U S A* 103:2641–2646. <http://dx.doi.org/10.1073/pnas.0511136103>.
- Lorzate M, Sachsenheimer T, Glass B, Habermann A, Gerl MJ, Kräusslich H-G, Brügger B. 2013. Comparative lipidomics analysis of HIV-1 particles and their producer cell membrane in different cell lines. *Cell Microbiol* 15:292–304. <http://dx.doi.org/10.1111/cmi.12101>.
- Ono A, Freed EO. 2001. Plasma membrane rafts play a critical role in HIV-1 assembly and release. *Proc Natl Acad Sci U S A* 98:13925–13930. <http://dx.doi.org/10.1073/pnas.241320298>.
- Ono A. 2010. Relationships between plasma membrane microdomains and HIV-1 assembly. *Biol Cell* 102:335–350. <http://dx.doi.org/10.1042/BC20090165>.
- Hogue IB, Grover JR, Soheilian F, Nagashima K, Ono A. 2011. Gag induces the coalescence of clustered lipid rafts and tetraspanin-enriched microdomains at HIV-1 assembly sites on the plasma membrane. *J Virol* 85:9749–9766. <http://dx.doi.org/10.1128/JVI.00743-11>.
- Freed EO, Martin MA. 2013. Human immunodeficiency viruses: replication, p 1502–1560. *In* Knipe DM, Howley PM (ed), *Fields virology*. Wolters Kluwer, Philadelphia, PA.
- Mariani C, Desdouts M, Favard C, Benaroch P, Muriaux DM. 2014. Role of Gag and lipids during HIV-1 assembly in CD4⁺ T cells and macrophages. *Front Microbiol* 5:312. <http://dx.doi.org/10.3389/fmicb.2014.00312>.
- Ehrlich LS, Fong S, Scarlata S, Zybarth G, Carter C. 1996. Partitioning of HIV-1 Gag and Gag-related proteins to membranes. *Biochemistry* 35: 3933–3943. <http://dx.doi.org/10.1021/bi952337x>.
- Hamard-Peron E, Muriaux D. 2011. Retroviral matrix and lipids, the intimate interaction. *Retrovirology* 8:15. <http://dx.doi.org/10.1186/1742-4690-8-15>.
- Saad JS, Miller J, Tai J, Kim A, Ghanam RH, Summers MF. 2006. Structural basis for targeting HIV-1 Gag proteins to the plasma membrane for virus assembly. *Proc Natl Acad Sci U S A* 103:11364–11369. <http://dx.doi.org/10.1073/pnas.0602818103>.
- Vlach J, Saad JS. 2013. Trio engagement via plasma membrane phospholipids and the myristoyl moiety governs HIV-1 matrix binding to bilayers. *Proc Natl Acad Sci U S A* 110:3525–3530. <http://dx.doi.org/10.1073/pnas.1216655110>.

28. Tang C, Loeliger E, Luncsford P, Kinde I, Beckett D, Summers MF. 2004. Entropic switch regulates myristate exposure in the HIV-1 matrix protein. *Proc Natl Acad Sci U S A* 101:517–522. <http://dx.doi.org/10.1073/pnas.0305665101>.
29. McGillivray DJ, Valincius G, Vanderah DJ, Febo-Ayala W, Woodward JT, Heinrich F, Kasianowicz JJ, Lösche M. 2007. Molecular-scale structural and functional characterization of sparsely tethered bilayer lipid membranes. *Biointerphases* 2:21–33. <http://dx.doi.org/10.1116/1.2709308>.
30. Schasfoort RB, AJ Tudos (ed). 2008. Handbook of surface plasmon resonance. Royal Society of Chemistry, Cambridge, United Kingdom.
31. Budvytyte R, Valincius G, Niaura G, Voiciuk V, Mickevicius M, Chapman H, Goh HZ, Shekhar P, Heinrich F, Shenoy SS, Lösche M, Vanderah DJ. 2013. Structure and properties of tethered bilayer lipid membranes with unsaturated anchor molecules. *Langmuir* 29:8645–8656. <http://dx.doi.org/10.1021/la401132c>.
32. Shenoy S, Moldovan R, Fitzpatrick J, Vanderah DJ, Deserno M, Lösche M. 2010. In-plane homogeneity and lipid dynamics in tethered bilayer lipid membranes (tBLMs). *Soft Matter* 6:1263–1274. <http://dx.doi.org/10.1039/b919988h>.
33. Valincius G, McGillivray DJ, Febo-Ayala W, Vanderah DJ, Kasianowicz JJ, Lösche M. 2006. Enzyme activity to augment the characterization of tethered bilayer membranes. *J Phys Chem B* 110:10213–10216. <http://dx.doi.org/10.1021/jp0616516>.
34. Budvytyte R, Mickevicius M, Vanderah DJ, Heinrich F, Valincius G. 2013. Modification of tethered bilayers by phospholipid exchange with vesicles. *Langmuir* 29:4320–4327. <http://dx.doi.org/10.1021/la304613a>.
35. Barer R, Joseph S. 1954. Refractometry of living cells. I. Basic principles. *Q J Microsc Sci* 3:399–423.
36. Benesch J, Askendal A, Tengvall P. 2000. Quantification of adsorbed human serum albumin at solid interfaces: a comparison between radioimmunoassay (RIA) and simple null ellipsometry. *Colloids Surf B* 18:71–81. [http://dx.doi.org/10.1016/S0927-7765\(99\)00136-8](http://dx.doi.org/10.1016/S0927-7765(99)00136-8).
37. Shenoy S, Shekhar P, Heinrich F, Daou M-C, Gericke A, Ross AH, Lösche M. 2012. Membrane association of the PTEN tumor suppressor: Molecular details of the protein-membrane complex from SPR binding studies and neutron reflection. *PLoS One* 7:e32591. <http://dx.doi.org/10.1371/journal.pone.0032591>.
38. Nanda H, Datta SAK, Heinrich F, Lösche M, Rein A, Krueger S, Curtis JE. 2010. Electrostatic interactions and binding orientation of HIV-1 matrix, studied by neutron reflectivity. *Biophys J* 99:2516–2524. <http://dx.doi.org/10.1016/j.bpj.2010.07.062>.
39. Weise K, Huster D, Kapoor S, Triola G, Waldmann H, Winter R. 2013. Gibbs energy determinants of lipoprotein insertion into lipid membranes: the case study of Ras proteins. *Faraday Discuss* 161:549–561. <http://dx.doi.org/10.1039/C2FD20100C>.
40. Dick RA, Goh SL, Feigenson GW, Vogt VM. 2012. HIV-1 Gag protein can sense the cholesterol and acyl chain environment in model membranes. *Proc Natl Acad Sci U S A* 109:18761–18766. <http://dx.doi.org/10.1073/pnas.1209408109>.
41. Feigenson GW. 2007. Phase boundaries and biological membranes. *Annu Rev Biophys Biomol Struct* 36:63–77. <http://dx.doi.org/10.1146/annurev.biophys.36.040306.132721>.
42. Lingwood D, Simons K. 2010. Lipid rafts as a membrane-organizing principle. *Science* 327:46–50. <http://dx.doi.org/10.1126/science.1174621>.
43. Pan J, Mills TT, Tristram-Nagle S, Nagle JF. 2008. Cholesterol perturbs lipid bilayers nonuniversally. *Phys Rev Lett* 100:198103. <http://dx.doi.org/10.1103/PhysRevLett.100.198103>.
44. Gerber PP, Cabrini M, Jancic C, Paoletti L, Banchio C, von Bilderling C, Sigaut L, Pietrasanta LI, Duette G, Freed EO, Gd Basile S, Moita CF, Moita LF, Amigorena S, Benaroch P, Geffner J, Ostrowski M. 2015. Rab27a controls HIV-1 assembly by regulating plasma membrane levels of phosphatidylinositol 4,5-bisphosphate. *J Cell Biol* 209:435–452. <http://dx.doi.org/10.1083/jcb.201409082>.
45. Kooijman EE, King KE, Gangoda M, Gericke A. 2009. Ionization properties of phosphatidylinositol polyphosphates in mixed model membranes. *Biochemistry* 48:9360–9371. <http://dx.doi.org/10.1021/bi9008616>.
46. Olety B, Veatch SL, Ono A. 2015. Phosphatidylinositol-(4,5)-bisphosphate acyl chains differentiate membrane binding of HIV-1 Gag from that of the phospholipase C δ 1 pleckstrin homology domain. *J Virol* 89:7861–7873. <http://dx.doi.org/10.1128/JVI.00794-15>.
47. Chertova E, Chertov O, Coren LV, Roser JD, Trubey CM, Bess JW, Sowder RC, Barsov E, Hood BL, Fisher RJ, Nagashima K, Conrads TP, Veenstra TD, Lifson JD, Ott DE. 2006. Proteomic and biochemical analysis of purified human immunodeficiency virus type 1 produced from infected monocyte-derived macrophages. *J Virol* 80:9039–9052. <http://dx.doi.org/10.1128/JVI.01013-06>.
48. Linde ME, Colquhoun DR, Ubaida Mohien C, Kole T, Aquino V, Cotter R, Edwards N, Hildreth JEK, Graham CR. 2013. The conserved set of host proteins incorporated into HIV-1 virions suggests a common egress pathway in multiple cell types. *J Proteome Res* 12:2045–2054. <http://dx.doi.org/10.1021/pr300918r>.
49. Bryant M, Ratner L. 1990. Myristoylation-dependent replication and assembly of human immunodeficiency virus 1. *Proc Natl Acad Sci U S A* 87:523–527. <http://dx.doi.org/10.1073/pnas.87.2.523>.
50. Göttlinger HG, Sodroski JG, Haseltine WA. 1989. Role of capsid precursor processing and myristoylation in morphogenesis and infectivity of human immunodeficiency virus type 1. *Proc Natl Acad Sci U S A* 86:5781–5785. <http://dx.doi.org/10.1073/pnas.86.15.5781>.
51. O'Carroll IP, Crist RM, Mirro J, Harvin D, Soheilian F, Kamata A, Nagashima K, Rein A. 2012. Functional redundancy in HIV-1 viral particle assembly. *J Virol* 86:12991–12996. <http://dx.doi.org/10.1128/JVI.06287-11>.
52. Rein A, McClure MR, Rice NR, Luftig RB, Schultz AM. 1986. Myristoylation site in Pr65gag is essential for virus particle formation by Moloney murine leukemia virus. *Proc Natl Acad Sci U S A* 83:7246–7250. <http://dx.doi.org/10.1073/pnas.83.19.7246>.
53. Zhou W, Resh MD. 1996. Differential membrane binding of the human immunodeficiency virus type 1 matrix protein. *J Virol* 70:8540–8548.
54. Kempf N, Postupalenko V, Bora S, Didier P, Arntz Y, de Rocquigny H, Mély Y. 2015. The HIV-1 nucleocapsid protein recruits negatively charged lipids to ensure its optimal binding to lipid membranes. *J Virol* 89:1756–1767. <http://dx.doi.org/10.1128/JVI.02931-14>.
55. Datta SAK, Heinrich F, Raghunandan S, Krueger S, Curtis JE, Rein A, Nanda H. 2011. HIV-1 Gag extension: conformational changes require simultaneous interaction with membrane and nucleic acid. *J Mol Biol* 406:205–214. <http://dx.doi.org/10.1016/j.jmb.2010.11.051>.
56. Fuller SD, Wilk T, Gowen BE, Kräusslich HG, Vogt VM. 1997. Cryo-electron microscopy reveals ordered domains in the immature HIV-1 particle. *Curr Biol* 7:729–738. [http://dx.doi.org/10.1016/S0960-9822\(06\)00331-9](http://dx.doi.org/10.1016/S0960-9822(06)00331-9).
57. Gheysen D, Jacobs E, de Foresta F, Thiriart C, Francotte M, Thines D, De Wilde M. 1989. Assembly and release of HIV-1 precursor Pr55gag virus-like particles from recombinant baculovirus-infected insect cells. *Cell* 59:103–112. [http://dx.doi.org/10.1016/0092-8674\(89\)90873-8](http://dx.doi.org/10.1016/0092-8674(89)90873-8).
58. Chukkappalli V, Hogue IB, Boyko V, Hu W-S, Ono A. 2008. Interaction between the human immunodeficiency virus type 1 Gag matrix domain and phosphatidylinositol-(4,5)-bisphosphate is essential for efficient Gag membrane binding. *J Virol* 82:2405–2417. <http://dx.doi.org/10.1128/JVI.01614-07>.
59. Chan J, Dick RA, Vogt VM. 2011. Rous sarcoma virus gag has no specific requirement for phosphatidylinositol-(4,5)-bisphosphate for plasma membrane association *in vivo* or for liposome interaction *in vitro*. *J Virol* 85:10851–10860. <http://dx.doi.org/10.1128/JVI.00760-11>.
60. Peitzsch RM, McLaughlin S. 1993. Binding of acylated peptides and fatty acids to phospholipid vesicles: pertinence to myristoylated proteins. *Biochemistry* 32:10436–10443. <http://dx.doi.org/10.1021/bi00090a020>.
61. Israelachvili J, Mitchell D, Ninham B. 1976. Theory of self-assembly of hydrocarbon amphiphiles into micelles and bilayers. *J Chem Soc Faraday Trans* 72:1525–1568. <http://dx.doi.org/10.1039/f29767201525>.
62. Heinrich F, Nanda H, Goh HZ, Bachert C, Lösche M, Linstedt AD. 2014. Myristoylation restricts orientation of the GRASP domain on membranes and promotes membrane tethering. *J Biol Chem* 289:9683–9691. <http://dx.doi.org/10.1074/jbc.M113.543561>.
63. Alfadhli A, Still A, Barklis E. 2009. Analysis of human immunodeficiency virus type 1 matrix binding to membranes and nucleic acids. *J Virol* 83:12196–12203. <http://dx.doi.org/10.1128/JVI.01197-09>.
64. Anraku K, Fukuda R, Takamune N, Misumi S, Okamoto Y, Otsuka M, Fujita M. 2010. Highly sensitive analysis of the interaction between HIV-1 Gag and phosphoinositide derivatives based on surface plasmon resonance. *Biochemistry* 49:5109–5116. <http://dx.doi.org/10.1021/bi9019274>.
65. Vlach J, Saad JS. 2015. Structural and molecular determinants of HIV-1 Gag binding to the plasma membrane. *Front Microbiol* 6:232. <http://dx.doi.org/10.3389/fmicb.2015.00232>.
66. Graber ZE, Jiang Z, Gericke A, Kooijman EE. 2012. Phosphatidylinositol-4,5-bisphosphate ionization and domain formation in the presence of

- lipids with hydrogen bond donor capabilities. *Chem Phys Lipids* 165:696–704. <http://dx.doi.org/10.1016/j.chemphyslip.2012.07.003>.
67. Kučerka, N, Tristram-Nagle S, Nagle JF. 2005. Structure of fully hydrated fluid-phase lipid bilayers with monounsaturated chains. *J Membr Biol* 208:193–202.
 68. Hung W-C, Lee M-T, Chen F-Y, Huang HW. 2007. The condensing effect of cholesterol in lipid bilayers. *Biophys J* 92:3960–3967. <http://dx.doi.org/10.1529/biophysj.106.099234>.
 69. Stillwell W, Ehringer WD, Dumaual AC, Wassall SR. 1994. Cholesterol condensation of α -linolenic and γ -linolenic acid-containing phosphatidylcholine monolayers and bilayers. *Biochim Biophys Acta* 1214:131–136. [http://dx.doi.org/10.1016/0005-2760\(94\)90036-1](http://dx.doi.org/10.1016/0005-2760(94)90036-1).
 70. de Meyer F, Smit B. 2009. Effect of cholesterol on the structure of a phospholipid bilayer. *Proc Natl Acad Sci U S A* 106:3654–3658. <http://dx.doi.org/10.1073/pnas.0809959106>.
 71. Pan J, Tristram-Nagle S, Nagle JF. 2009. Effect of cholesterol on structural and mechanical properties of membranes depends on lipid chain saturation. *Phys Rev E Stat Nonlin Soft Matter Phys* 80(Pt 1):021931.
 72. Pandit SA, Chiu S-W, Jakobsson E, Grama A, Scott HL. 2008. Cholesterol packing around lipids with saturated and unsaturated chains: a simulation study. *Langmuir* 24:6858–6865. <http://dx.doi.org/10.1021/la8004135>.
 73. Dahl CE. 1981. Effect of sterol structure on acyl chain ordering in phosphatidylcholine vesicles: a deuterium nuclear magnetic resonance and electron spin resonance study. *Biochemistry* 20:7158–7161. <http://dx.doi.org/10.1021/bi00528a016>.
 74. Pöyry S, Róg T, Karttunen M, Vattulainen I. 2008. Significance of cholesterol methyl groups. *J Phys Chem B* 112:2922–2929. <http://dx.doi.org/10.1021/jp7100495>.
 75. Simons K, Ehehalt R. 2002. Cholesterol, lipid rafts, and disease. *J Clin Invest* 110:597–603. <http://dx.doi.org/10.1172/JCI0216390>.
 76. Lindwasser OW, Resh MD. 2002. Myristoylation as a target for inhibiting HIV assembly: unsaturated fatty acids block viral budding. *Proc Natl Acad Sci U S A* 99:13037–13042. <http://dx.doi.org/10.1073/pnas.212409999>.
 77. Ono A, Waheed AA, Freed EO. 2007. Depletion of cellular cholesterol inhibits membrane binding and higher-order multimerization of human immunodeficiency virus type 1 Gag. *Virology* 360:27–35. <http://dx.doi.org/10.1016/j.virol.2006.10.011>.
 78. Charlier L, Louet M, Chaloin L, Fuchs P, Martinez J, Muriaux D, Favard C, Floquet N. 2014. Coarse-grained simulations of the HIV-1 matrix protein anchoring: revisiting its assembly on membrane domains. *Biophys J* 106:577–585. <http://dx.doi.org/10.1016/j.bpj.2013.12.019>.
 79. Jiang Z, Redfern RE, Isler Y, Ross AH, Gericke A. 2014. Cholesterol stabilizes fluid phosphoinositide domains. *Chem Phys Lipids* 182:52–61. <http://dx.doi.org/10.1016/j.chemphyslip.2014.02.003>.
 80. Kerviel A, Thomas A, Chaloin L, Favard C, Muriaux D. 2013. Virus assembly and plasma membrane domains: which came first? *Virus Res* 171:332–340. <http://dx.doi.org/10.1016/j.virusres.2012.08.014>.
 81. Dalton AK, Murray PS, Murray D, Vogt VM. 2005. Biochemical characterization of Rous sarcoma virus MA protein interaction with membranes. *J Virol* 79:6227–6238. <http://dx.doi.org/10.1128/JVI.79.10.6227-6238.2005>.